Volume 9, Issue 1, 092506 (1-10)

Signal Processing and Renewable Energy (SPRE)

https://doi.org/10.57647/j.spre.2025.0901.06

Image segmentation enhancement using aggregated kernel graph cut

Yasin Ghasemipour, Mehrnaz Niazi*

Department of Computer Engineering, Pishtazan Higher Education Institute, Shiraz, Iran.

***Corresponding author:** m.niazi@pishtazan.ac.ir

Original Research

Received:
30 December 2024
Revised:
9 January 2025
Accepted:
25 February 2025
Published online:
1 March 2025

Abstract:

Kernel graph cut-based image segmentation techniques have proven useful in processing image data; yet, they frequently face limits when addressing intricate image structures due to inherent constraints. The traditional kernel graph cut technique is constrained in its capacity to manage complicated image structures due to its inadequacy in capturing intricate image features. This research tackles these issues by presenting a novel method that consolidates spatial and intensity data within a kernel structure. The methodology presents a novel kernel structure that integrates spatial and intensity data, producing maps that illustrate variations in pixel intensity and spatial correlations. These maps facilitate the creation of a thorough similarity matrix. Utilizing the RBF kernel enhances data mapping, hence improving the effectiveness of the similarity matrix. This aggregated approach overcomes the limitations of conventional kernel graph cut approaches. This augmentation markedly improves the Dice coefficient and accuracy of image segmentation, especially in contexts with intricate image structures and varied intensity distributions. The proposed methodology was assessed utilizing photos from the Berkeley and Pascal datasets, in addition to a real and synthetic dataset that we produced. The results demonstrate exceptional performance, attaining a 99.40% Dice similarity, exceeding conventional energy-based approaches.

Keywords: Image segmentation; Energy-based methods; Graph cut; Intensity information; Spatial information; Radial based function

1. Introduction

In the domain of machine vision, image segmentation is now universally recognized as a crucial step in image preprocessing [1]. Image segmentation has numerous applications across various domains, including clinical imaging and object recognition.[2–4]. Among the commonly used methods for image segmentation are energy-based approaches [5–7]. These methods are generally divided into two main categories: continuous and discrete [8]. Methods for continuous segmentation Regard image segmentation as an issue within the continuous domain [8]. In this context, approaches such as Active Contours and Level Sets can be presented. Active Contour methods employ a variety of techniques, for example, the snake model [9], balloon model [10], and geometric active contours [11]. Generally, these methods excel in various domains due to their energy function minimization [7]. However, Active Contour methods may not support topological changes [12]. Furthermore, they often struggle with inhomogeneous image segmentation and are highly sensitive to initializations [13]. Level Set methods are a subset of Active Contour models, based on curve evolution [14]. In general, Level Set segmentation methods can perform segmentation based on edge information [15] or region-based information [16]. These methods offer more flexibility concerning the topology of images [14]. However, they are sensitive to image intensity inhomogeneity and noise [17]. On the other hand, to address the shortcomings of these methods, a combination of edge-based and region-based approaches can be employed. Nevertheless, this process also requires determining fusion coefficients [12].

Discrete segmentation techniques function within a discrete domain. Techniques like graph cut approaches has the capacity to enhance performance and efficiency [8]. Research conducted in this field can be categorized into three main approaches: 1) Input Feature Approach, 2) Energy Function Approach, and 3) Kernel Approach.

In the first approach, input features can encompass any photometric characteristics from the image, such as intensity, differences, color, or texture [8]. For instance, in the paper [18], for the classification of skin lesions, they initially employ a graph-based segmentation method. Using this

approach, the model's input feature is just each pixel's intensity in the color space of HSV (Hue, Saturation, Value). In the paper [19], the segmentation algorithm is based on semantic image information. In this approach, information such as color, texture, and spatial data is utilized. In the graph cut section, an Ultra-Metric Contour Map is used to calculate edge weights. While this method provides satisfactory performance, it may not perform well in image regions where the background and object share strong color similarity. In the paper [20], an optimal method for depth estimation is presented using graph cut optimization and superpixel segmentation. In this method, a set of similar pixels is utilized for depth estimation. Features such as position, color, and brightness are used as attributes for each node in the graph, essentially constructing each superpixel from this information. Additionally, by incorporating spatial gradients into cost function components, the method reduces discontinuities and spatial similarities in the results. This approach exhibits lower complexity compared to other methods in this field. In the paper [21], an optimal and precise segmentation method based on graph cut techniques is presented for 4D light field images. These images impose a significant computational burden due to their large data volume. This method utilizes superpixels to incorporate information such as appearance, location, and disparities into the energy function. In the case of 4D light field images, both spatial dimensions and angular dimensions are considered within the superpixels. Moreover, the use of superpixels reduces the computational load when working with hypergraphs. Ultimately, the hypergraph created is cut employing the graph cut method to obtain the desired segmentation. The effectiveness of this method is somewhat dependent on the quality of the LFSP (light field superpixels), which can reduce the algorithm's performance under certain conditions. For instance, when miniature objects have significant resemblance to the background.

In the second approach, the paper [22] introduces a novel method for motion compensation based on event-based motion segmentation. This method utilizes graph cut to achieve results with global consistency and local coherence. The designed energy function is a combination of the Potts function and the minimum descriptor length (MDL) principle. This energy function can accurately identify optimal data minima and deliver a segmentation with minimized fragments, ensuring both temporal and spatial smoothness. Nevertheless, the intricacy of this approach has grown more complex [23]. The Paper [24], Improved cervical cancer cell image segmentation holistically. It first uses an Input Feature Approach to preprocess input images for segmentation using adaptive anisotropic filters and morphological transformations. Second, it uses the Neutrosophic C-Means Clustering Technique (NCMCT) to measure indeterminacy across intensity classes and integrate energy functions into segmentation. It uses a Gaussian Distribution-based Kernel function to reduce ambiguity and improve neighborhood smoothing. A thorough approach to improving the cervical cancer cell image segmentation method improves accuracy and reliability.

In the paper [25], a Hessian filter is applied to CTCA (Computed Tomography Coronary Angiogram) images before graph-based lumen segmentation. We determine the vessel directions in each voxel after extracting feature vectors. The segmentation phase uses this directional information and gives the energy function an anisotropic component. This component improves lumen segmentation over classical methods. However, this method may miss small vessel lesions [26]. At [27] authors' work introduces significant algorithmic enhancements by incorporating rank constraints and penalty terms in their graph partitioning optimization algorithm. By leveraging the Laplacian matrix's eigenvalues, they achieve more precise segmentation results, enhancing the algorithm's effectiveness.

In the third approach, for example, in the paper [28], a RBF (Radial Basis Function) kernel is employed to improve data separation. By obtaining energy components in both spatial and spectral domains. utilizing the α–β-swap algorithm [29], segmentation is performed. Unlike algorithms based on Markov Random Fields and other spectral-spatial techniques, this technique performs well in terms of the accuracy of classification and region uniformity. According to the paper, further research and measurements are needed in the areas of spatial similarity and class separation. The article [30] improved cervical cancer cell image segmentation holistically. It first uses an Input Feature Approach to preprocess input images for segmentation using adaptive anisotropic filters and morphological transformations. Second, it uses the Neutrosophic C-Means Clustering Technique (NCMCT) to measure indeterminacy across intensity classes and integrate energy functions into segmentation. It uses a Gaussian Distribution-based Kernel function to reduce ambiguity and improve neighborhood smoothing. A thorough approach to improving the cervical cancer cell image segmentation method improves accuracy and reliability. In the paper [31], two kernels segment Positron Emission Tomography and Computed Tomography images. This technique enhances graphs through a two-step process. The optimization of the energy function commences with the RBF kernel. In the subsequent step, sigmoid, hyperbola, and polynomial kernels are employed to identify the optimal labels, and the outcomes are evaluated against one another. Optimal outcomes are derived from RBF and polynomial kernels. According to [32], due to the implementation of the method on fused images, the relationships between the images' asymmetric properties are disregarded. This action leads to a reduction in the method's performance.

In [33], The authors propose the "Energy Function Methodology" for natural image segmentation. They propose an innovative "adaptive fusion affinity graph" to minimize segmentation energy in noisy data. The "Kernel Approach" is enhanced by an advanced kernel density estimation technique, which refines image region similarity assessments. This technique enhances the efficiency and precision of image segmentation.

The Kernel Graph Cut algorithm utilizes solely pixel intensity values as input for the kernel. This method, while effective, may produce suboptimal results when the image subject exhibits significant shadows, and it is incapable of delivering accurate segmentation based solely on image in-

tensity. To address this challenge, a spatial factor is added to the RBF kernel [8]. With this approach, in addition to pixel intensity, the spatial location of pixels also affects the image segmentation. This allows the Kernel Graph Cut algorithm to perform better in segmenting images that have side effects and contain spatially coherent structures. In the following sections, the Kernel Graph Cut method will be discussed in section 2. In section 3, the spatial Kernel Graph Cut algorithm will be explored. The experimental findings will be presented in the fourth section, and the paper's conclusion will be given in section 5.

2. Graph cut method with RBF kernel

Kernel graph cut approaches improve conventional graph-based segmentation by utilizing kernel functions to project image features into a higher-dimensional space, facilitating the separation of intricate structures. This method represents an image as a weighted network, with nodes representing pixels and edges indicating similarity based on feature correlations [34]. The segmentation issue is addressed by max-flow/min-cut algorithms, with edge weights representing pipe capacities in a flow network [35]. The application of a kernel function, such as the Radial Basis Function (RBF) kernel, enhances the segmentation process by facilitating better differentiation across regions, particularly when pixel intensity is inadequate. This technique is very effective for managing intricate textures, lighting discrepancies, and irregular object edges [8].

In general, an image represents a spatial domain that is defined by an array Ω. The image for each pixel p is defined as $I_p = I(p) \in \mathscr{I}$. $\mathscr{I}$ is a subset of real numbers and can represent any image feature, such as intensity, color, or texture. The function λ will determine the label l for each pixel. $\mathscr{L}$ is the set of all labels, denoted as $\lambda(p) \in \mathscr{L}$ and R_l is defined as the set of pixels for each segment, denoted as $R_l = \{p \in \Omega | \lambda(p) = l\}$. The number of elements in L is represented by N_{reg}, which will be the quantity of the image segments.

$$\mathscr{F}(\lambda) = \mathscr{D}(\lambda) + \alpha \mathscr{R}(\lambda) \tag{1}$$

The Kernel Graph Cut method, according to equation (1), uses a function with two terms to describe and compute image features and boundaries [8]. One is data term, which assesses the adherence of each image segment to a statistical model, and the other is an element of regularization that produces smoother boundaries.

$\mathscr{F}$ is a segmentation function, $\mathscr{D}$ is the data term, $\mathscr{R}$ is the regularization term, and α is a constant coefficient governing segmentation smoothness. The data term in image segmentation is a maximum a posteriori (MAP) probability [36] problem. To achieve this, the likelihood of image data conditioned on each region, denoted as $P(I_p|R_l)$, is utilized. In terms of the MAP formulation, equation (2) can be used for defining the data term.

$$\mathscr{D}(\lambda) = \sum_{l \in \mathscr{L}} \sum_{p \in R_l} -\log P(I_p|R_l) \tag{2}$$

The piecewise constant segmentation model is a specific instance of the Gaussian distribution. due to the subsequent techniques being computationally straightforward. Let the model parameter of the region be piecewise constant [8]. The data term is defined as equation (3).

$$\mathscr{D}(\lambda) = \sum_{l \in \mathscr{L}} \sum_{p \in R_l} (\mu_l - I_p)^2 \tag{3}$$

The data has been delineated employing a kernel within a graph cut methodology to enhance its separation. Mercer's theory focuses on the implicit mapping of data. According to Mercer's theory, any function that is symmetric and semi-definite positive can represent inner products of data in a space in higher dimensions [37]. This operation greatly decreases computing complexity [8, 38]. The transformation function ϕ in the kernel performs the mapping of data to a higher-dimensional space which is formulated according to equation (4).

$$K(\mathbf{x}, \mathbf{y}) = \phi(\mathbf{x})^{\mathbf{T}} \cdot \phi(\mathbf{y}) \tag{4}$$

where x and y are input parameters. The RBF kernel [8], represented as $K(x,y) = \exp(-||x-y||^2/2\sigma^2)$, is a commonly utilized kernel function that quantifies the similarity or distance between two data points, x and y, using Euclidean distance. The free parameter σ in this kernel regulates how each data point's influence is perceived. While mapping the data with the RBF kernel [8] to a higher-dimensional space, the data term is defined as demonstrated in equation (5) [39].

$$\begin{aligned} D_{\text{RBF}}(I_p, \mu) &= ||\phi(I_p) - \phi(\mu)||^2 \\ &= (\phi(I_p) - \phi(\mu))^T \cdot (\phi(I_p) - \phi(\mu)) \\ &= \phi(I_p)^T \phi(I_p) - \phi(\mu)^T \phi(I_p) \\ &- \phi(I_p)^T \phi(\mu) + \phi(\mu)^T \phi(\mu) \\ &= K(I_p, I_p) + K(\mu, \mu) - 2K(I_p, \mu) \\ &= 2 - 2K(I_p, \mu), \mu \in \{\mu_l\}_{1 \le l \le N_{reg}} \end{aligned} \tag{5}$$

In order to smooth the boundaries, the regularization term is used. The following term is defined for boundary pixels p and its 4 horizontal and vertical neighbors q as shown in equation (6) [8]. The const component is a constant value used to control the smoothing.

$$\mathscr{R}(\lambda) = \min(const^2, |\mu_{\lambda(p)} - \mu_{\lambda(q)}|^2) \tag{6}$$

The optimization process is performed in two steps at each iteration. In the first step, the goal is to optimize the energy function according to the factors of each region. In other words, the factor specific to each region is the statistical parameter μ_l. In the subsequent stage, kernel graph cut methods are employed with the energy graph to implement a minimum cut, yielding the image segmentation.

3. Aggregated kernel graph cut algorithm

K-means clustering is a key unsupervised learning approach in data analysis, esteemed for its simplicity and computing effectiveness [40]. The algorithm's main objective is to categorize input data points into various classes according to their intrinsic distances from one another, a concept initially presented by MacQueen [41]. K-means clustering was chosen as the preliminary phase of our approach for categorizing data points based on intrinsic distances, owing

to its simplicity and computational efficiency, prior to implementing kernel graph cuts for enhanced segmentation. In this study, an aggregated kernel leveraging pixel intensity and spatial information is employed to enhance the accuracy of the segmentation process. This approach demonstrates exceptional efficacy, especially in scenarios where images encompass objects with diverse intensities and intricate spatial layouts. The methodology revolves around two pivotal components: the utilization of the Radial Basis Function (RBF) kernel [8], and the incorporation of the graph cut algorithm.

$$\mathscr{D}_{Int}(\lambda) = \sum_{l\in\mathscr{L}} \sum_{p\in R_l} (\mu_l - I_p)^2 \tag{7}$$

These constituents operate synergistically, establishing a robust segmentation framework that effectively exploits both pixel intensity and spatial interconnections among pixels. In order to construct an aggregated RBF kernel, an intensity-based difference map $\mathscr{D}_{Int}$ is generated by computing the differences between pixel values and the reference value for each region, as described by equation (7) [39].

$$\mathscr{D}_{Spt}(\lambda) = \sum_{l\in\mathscr{L}}^{ij} \sum_{p\in R_l}^{ij} \min(|i_{\mu_l} - i_{I_p}|, |j_{\mu_l} - j_{I_p}|) \tag{8}$$

Then, a spatial-based difference map $\mathscr{D}_{Spt}$ is constructed by calculating the minimum of the absolute differences between pixel coordinates and the coordinates of the central reference point, as described by equation (8), and it is normalized. This map captures the spatial proximity of each pixel to its center.
where i and j represent spatial positions in the image. A full similarity matrix is generated by integrating the intensity-based difference map with the spatial proximity map, yielding more thorough information regarding the differences in the image. The data corresponds based on the RBF kernel in order to more effectively separate the data in the graph cut method. This method provides a strong framework for precise image segmentation that can be applied to various types of images and conditions. Equation (9) represents the aggregated data mapping based on both intensity and spatial proximity using the RBF kernel.

$$\begin{aligned} D_{\text{RBF}}(\mathscr{D}_{Int}, \mathscr{D}_{Spt}) &= ||\phi(\mathscr{D}_{Int}) + \phi(\mathscr{D}_{Spt})||^2 \\ &= (\phi(\mathscr{D}_{Int}) + \phi(\mathscr{D}_{Spt}))^T \cdot (\phi(\mathscr{D}_{Int}) + \phi(\mathscr{D}_{Spt})) \\ &= \phi(\mathscr{D}_{Int})^T \phi(\mathscr{D}_{Int}) + \phi(\mathscr{D}_{Spt})^T \phi(\mathscr{D}_{Int}) \\ &+ \phi(\mathscr{D}_{Int})^T \phi(\mathscr{D}_{Spt}) + \phi(\mathscr{D}_{Spt})^T \phi(\mathscr{D}_{Spt}) \\ &= K(\mathscr{D}_{Int}, \mathscr{D}_{Int}) + K(\mathscr{D}_{Spt}, \mathscr{D}_{Spt}) + 2K(\mathscr{D}_{Int}, \mathscr{D}_{Spt}) \\ &= 2 + 2K(\mathscr{D}_{Int}, \mathscr{D}_{Spt}) \end{aligned} \tag{9}$$

The data term mapped with the RBF kernel incorporates not only intensity information but also spatial information into the image segmentation process. This allows the algorithm to consider the proximity of pixels to specified central points, potentially leading to more cohesive and meaningful segmentations. The integration of spatial information can be particularly useful when dealing with images containing spatially coherent structures, where spatial relationships between pixels are crucial for precise segmentation.

While smoothing the boundaries using the Regularization term, the optimization process with the intensity and spatial RBF kernel is performed in two stages at each iteration. In the first stage, the goal is to optimize the energy function according to the factors of each region, which are the statistical parameters μ_l. The second stage involves applying a minimum cut utilizing graph-cut algorithms and taking into account the energy graph's structure according to intensity and spatial data to produce the final segmentation. Algorithm 1 represents the aggregated kernel graph-cut algorithm.

4. Experimental results

One dataset composed of Berkeley [42] and Pascal [43] photos, a synthetic dataset, and a real-world dataset with objects that had intricate textures, shadows, and different hues were all utilized to assess the effectiveness of the suggested algorithm. In this work, 400 by 400 pixel images with 90 sets of the Berkeley and Pascal datasets, 80 sets of synthetic images, and 50 sets of real-color photos were all used to get experimental results. Six energy-based algorithms were used to compare the efficiency of the suggested approach, namely RBF [8], Customized RBF [44], AMOE (Appearance Model and Orientation Energy) [45], Bias Level Set [46], Krawtchouk [47], and L2S (Legendre Level Set) [48]. Using a set of six separate evaluation indicators,

Algorithm 1. Aggregated kernel graph-cut.

input: given image (*I*)
output: segmented image

procedure image segmentation
extract primary centers using K-means algorithm

repeat
define intensity data term ($\mathscr{D}_{Int}$) using equation (7)
define spatial data term ($\mathscr{D}_{Spt}$) using equation (8)
compute combined data term (D)

apply aggregated RBF kernel as per equation (9)
compute regularization term using equation (6)
compute graph energy function using equation (1)

construct image graph based on graph energy function
apply min-cut algorithm to segment the image

recalculate cluster centers based on segmentation

until cluster centers remain unchanged

return segmented image

end procedure

the suggested algorithm's performance was assessed which includes the Dice coefficient (DSC) [49], Jaccard index [50], Accuracy [51], PSNR (Peak Signal-to-Noise Ratio) [52], MSSD (Maximum Symmetric Surface Distance) [53] and Total Time (sec) are used. It is crucial to remember that the evaluations were carried out using the MATLAB 2020a program along with a CPU running at 4.20 GHz and 16 GB of RAM. On the website https://github.com/mehrnazniazi, you can discover the implementation of the suggested method.

4.1 Results on the Berkeley and Pascal dataset

To comprehensively evaluate the proposed algorithm, a laboratory study was conducted using two datasets, Pascal and Berkeley. In general, 90 JPEG images with dimensions of 400 by 400 pixels were randomly selected from these datasets. The Pascal and Berkeley datasets contain diverse and complex images with different classes and complexities. These datasets have been chosen as a valuable source for evaluating the algorithm's capabilities in the field of image segmentation. In figure 1 presents samples from the Pascal and Berkeley datasets. The first row presents images obtained from the Berkeley data set, whereas the following row displays images from the Pascal data set.
For quantitative evaluation, Table 1 represents the comparison of the results between the algorithms used on the Pascal and Berkeley datasets. A review of the table shows that the Dice metric in the proposed algorithm is 0.94% higher than the value in the RBF method. Similarly, the difference in the Jaccard metric is 1.76%, and in the Accuracy metric, it's 3.72%. The observed differences highlight a notable enhancement of the proposed algorithm compared to the RBF method in these metrics. Additionally, regarding the PSNR metric, the proposed algorithm shows an advantage of 3.32 units. The MSSD metric shows a difference of 0.01 units, indicating that the proposed method surpassed the RBF method in terms of outcomes. The proposed method ranks second in terms of execution speed.
Figure 2 displays samples of results from Pascal and Berkeley images. As observed, the proposed algorithm in the third column has provided better results compared to other algorithms and has effectively segmented the images. The suggested approach has improved background and foreground separation in complicated images by simultaneously leveraging brightness and spatial information. The RBF and Customized algorithms in the fourth and fifth columns, in images with more complex backgrounds containing texture and shadows, failed to segment the background effectively. The reason for this segmentation weakness is that these algorithms solely rely on brightness intensity as a feature and, therefore, couldn't perform well in complex images and regions with shadows. The Bias Level Set, L2S, Krawtchouk, and AMOE algorithms in columns six to nine also failed to effectively segment the foreground despite correctly identifying the background.

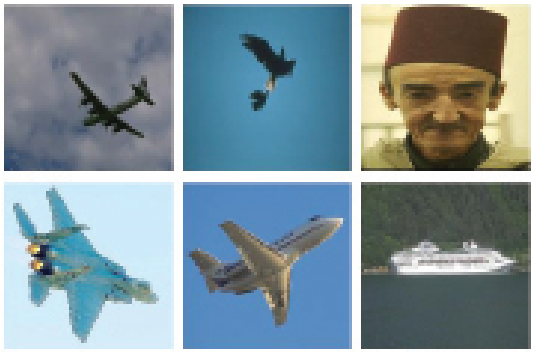

Figure 1. Pascal and Berkeley dataset samples.

4.2 Results on the synthetic dataset

To comprehensively evaluate the proposed algorithm, a laboratory study was conducted using a synthetic dataset. In general, this dataset consists of 70 JPEG images with dimensions of 400 by 400 pixels. The synthetic dataset was selected to include complex images with different textures and backgrounds. Figure 3 displays some examples from the synthetic dataset.
Table 2 compares the quantitative performance outcomes of the methods on the simulated dataset. The findings indicate that the proposed algorithm's Dice coefficient is 3.51% higher than the AMOE method's value. Additionally, there is a 6.32% difference in the Jaccard index and an 11.28% difference in Accuracy. These differences indicate a significant improvement of the proposed algorithm over AMOE and RBF in these metrics. Moreover, there is a 3.95-unit improvement in the PSNR metric in favor of the proposed algorithm. In the case of the MSSD metric, there is a dif-

Table 1. Comparing energy-based techniques using various criterion on a collection of Pascal and Berkeley datasets.

Algorithms	Evaluation metrics					
	DSC	Jaccard	accuracy	PSNR	MSSD	Total time(sec)
suggested approach	99.00	98.06	90.23	68.57	0.01	2.36
RBF	98.06	96.30	86.51	65.25	0.02	1.15
customized	97.47	95.21	82.03	63.80	0.03	4.34
bias level set	97.66	95.56	77.34	65.21	0.03	5.44
L2S	72.07	58.99	59.65	62.33	0.08	10.24
Krawtchouk	62.86	49.20	49.57	61.29	0.11	23.46
AMOE	90.54	84.19	51.66	59.48	0.14	4.70

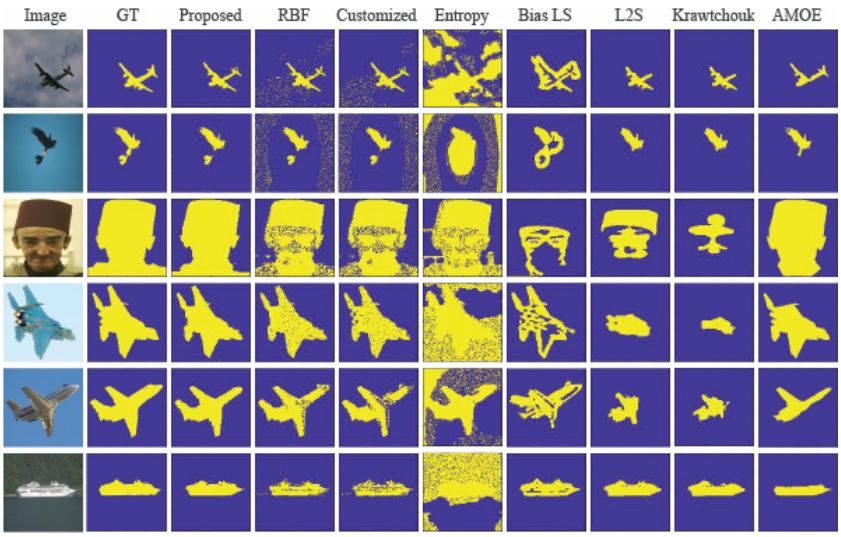

Figure 2. Rows comprise of original image, ground truth, suggested method, RBF method, customized RBF method, bias level set, L2S, Krawtchouk, and AMOE. Includes several assessments of Pascal and Berkeley images.

Figure 3. Synthetic dataset samples.

ference of 0.051 units, demonstrating that the suggested algorithm outperformed the AMOE approach in terms of results.

Figure 4 displays several samples of results from the synthetic images. As can be seen, the suggested method in the third column outperformed other algorithms in terms of outcomes. The RBF and Customized algorithms in the fourth and fifth columns couldn't separate the complex background from other parts of the image effectively. In columns six to nine, the Bias Level Set, L2S, Krawtchouk, and AMOE algorithms, despite detecting the background, couldn't segment the foreground accurately. The suggested algorithm's simultaneous utilization of intensity and location data accounts for its advantage. This approach utilizes a more comprehensive difference map for segmentation, resulting in better adjustment of the energy-based image graph and, consequently, improved performance of the graph cut algorithm.

4.3 Results on real dataset

Experimentation on the real dataset is also shown, along with evaluation results for the suggested approach. The real image dataset consists of 60 JPEG images with dimensions of 400 by 400 pixels. The real datasets have been chosen to include complex images with texture and shadows. Figure 5 displays some examples from the real image datasets.

In Table 3, a quantitative analysis of algorithm performance on the real dataset is presented. The outcomes show that the AMOE method's Dice coefficient is 1.46% lower than that of the suggested method. Additionally, there is a difference of 2.69% in the Jaccard index and 9.93% in the Accuracy

Table 2. Comparing energy-based techniques using various criterion on the synthetic dataset.

Algorithms	Evaluation metrics					
	DSC	Jaccard	accuracy	PSNR	MSSD	Total time(sec)
suggested approach	99.40	98.82	96.17	69.87	0.009	2.97
RBF	94.27	89.94	84.89	60.55	0.07	2.12
customized	92.77	87.36	80.25	59.37	0.09	1.44
bias level set	74.92	69.25	79.79	57.15	0.27	1.58
L2S	73.30	60.08	60.12	59.88	0.08	89
Krawtchouk	69.35	55.24	55.27	59.06	0.09	192.75
AMOE	95.89	92.50	78.65	65.92	0.06	6.01

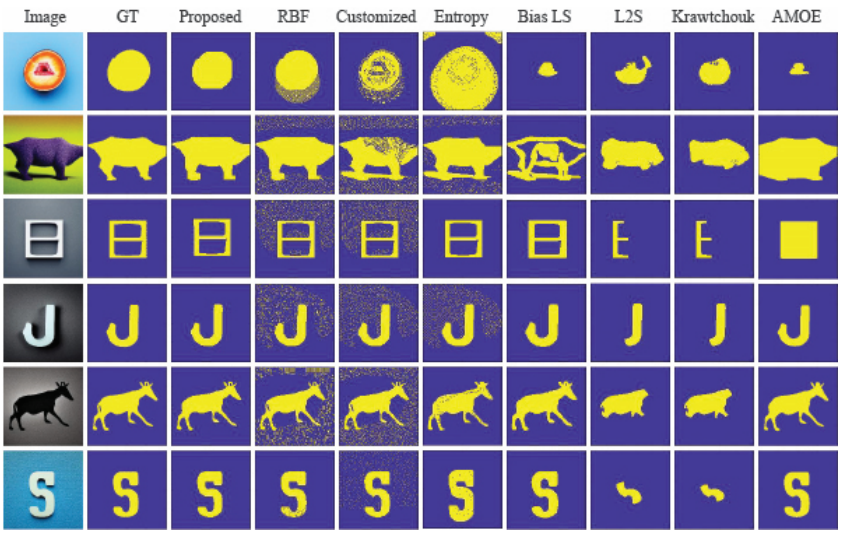

Figure 4. Rows comprise of original image, ground truth, suggested method, RBF method, customized RBF method, bias level set, L2S, Krawtchouk, and AMOE. Includes several assessments of synthetic images.

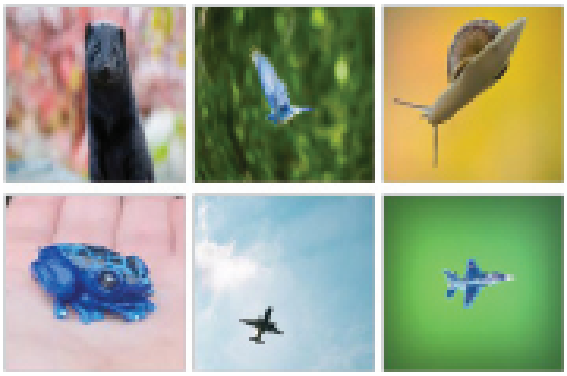

Figure 5. Real dataset samples.

metric. several variations show that the suggested algorithm has significantly improved over the second-best approach in several criteria. Moreover, in terms of PSNR, there is an enhancement of 3.30 units in the proposed algorithm. A difference of 0.02 units in the MSSD metric indicates that the suggested algorithm outperformed the AMOE approach in terms of results.

Figure 6 displays several samples of results on the real images. As observed, the proposed algorithm in the third column provides better image segmentation compared to other algorithms due to its simultaneous use of brightness and spatial maps. The RBF and Customized algorithms in the fourth and fifth columns fail to effectively separate complex backgrounds from foreground objects as they solely rely on image brightness. In the sixth to ninth columns, the Bias Level Set, L2S, Krawtchouk, and AMOE algorithms, despite their ability to detect background, struggle to accurately segment the foreground.

5. Conclusion

The Kernel Graph Cut algorithm represents a significant approach within the realm of energy-based image segmentation techniques. It fundamentally relies on edge detection and the separation of objects in images, achieved through the analysis of connected graphs. However, drawbacks such as sensitivity to illumination variations, difficulties in detecting objects with different intensities, and complex spatial arrangements limit its applicability to complex and diverse images. This research proposes a novel method for segmenting images that effectively uses both spatial and intensity data. This approach leverages the benefits

Table 3. Comparing energy-based techniques using various criterion on the real dataset.

Algorithms	Evaluation metrics					
	DSC	Jaccard	accuracy	PSNR	MSSD	Total time (sec)
suggested approach	99.17	98.38	93.27	69.51	0.01	2.3
RBF	92.39	87.89	83.34	63.27	0.11	1.56
customized	91.75	86.50	77.51	61.19	0.12	3.53
bias level set	87.04	78.87	43.65	59.04	0.20	4.79
L2S	70.46	60.59	61.25	64.00	0.06	93.95
Krawtchouk	66.80	54.39	54.51	62.16	0.08	197.35
AMOE	97.71	95.69	67.61	66.21	0.03	5.77

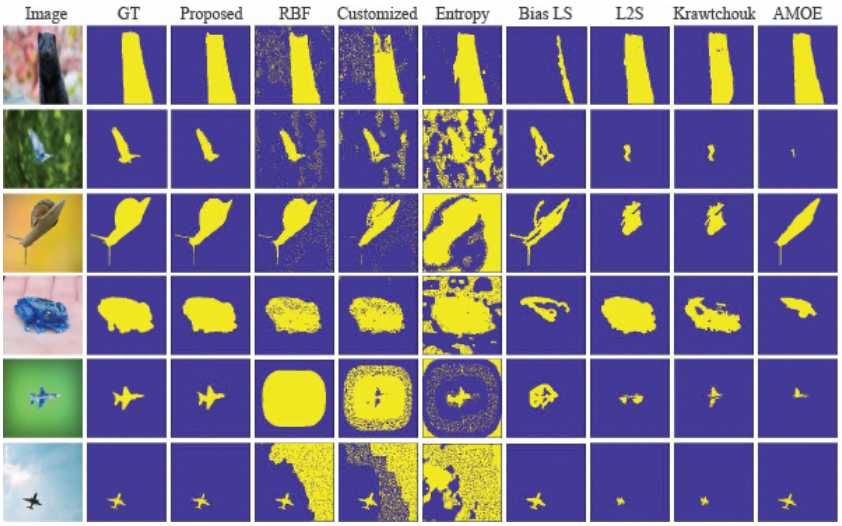

Figure 6. Rows comprise of original image, ground truth, suggested method, RBF method, customized RBF method, bias level set, L2S, Krawtchouk, and AMOE. Includes several assessments of real images.

of kernel space, focusing on the objective function that incorporates the statistical deviation of intensity and spatial data for each region in the segmented image, as well as a regularization term to ensure smooth boundaries. The experimental results indicate that this method, utilizing an enhanced similarity matrix through the RBF kernel, has markedly improved the image segmentation process.

One of this approach's most significant benefits is its higher accuracy in detecting objects with different intensities and complex spatial arrangements. With an improvement of approximately 94% in the final results, this approach not only overcomes the limitations of the Kernel Graph Cut algorithm but also demonstrates its potential strength in solving image segmentation problems with diverse complexities and various challenges in image data. In future efforts, additional improvements can be implemented in this methodology by fine-tuning the application of intensity and spatial characteristics within each area, while considering the uniformity of regions. This may entail creating more advanced approaches for dynamic feature weighting and selection, allowing the algorithm to adjust to the unique traits of various image areas and possibly enhancing segmentation precision and reliability.

Authors contributions
Authors have contributed equally in preparing and writing the manuscript.

Availability of data and materials
The data that support the findings of this study are available from the corresponding author upon reasonable request. The public datasets of this study are available in references [42, 43]. The author dataset that supports the findings of this study is available at https://github.com/mehrnazniazi.

Conflict of interests
The authors declare that they have no known competing financial interests or personal relationships that could have appeared to influence the work reported in this paper.

References

[1] M. Tang. "Image segmentation technology and its application in digital image processing.". *International Conference on Advance in Ambient Computing and Intelligence, ICAACI 2020, Institute of Electrical and Electronics Engineers Inc*, page 158–160, 2020. DOI: https://doi.org/10.1109/ICAACI50733.2020.00040.

[2] A. Niaz, E. Iqbal, A. A. Memon, A. Munir, J. Kim, and K. N. Choi. "Edge-based local and global energy active contour model driven by signed pressure force for image segmentation.". *IEEE Trans Instrum Meas*, 72:1–14, 2023. DOI: https://doi.org/10.1109/TIM.2023.3317481.

[3] P. N. Bui, D. T. Le, J. Bum, S. Kim, S. J. Song, and H. Choo. "Semi-supervised learning with fact-forcing for medical image segmentation.". *IEEE Access*, 11:99413–99425, 2023. DOI: https://doi.org/10.1109/ACCESS.2023.3313646.

[4] Y. Zhou et al. "Cyclic learning: Bridging image-level labels and nuclei instance segmentation.". *IEEE Trans Med Imaging*, 42(10): 3104–3116, 2023. DOI: https://doi.org/10.1109/TMI.2023.3275609.

[5] H. Zhu, J. Zhang, G. Xu, and L. Deng. "Tensor field graph-cut for image segmentation: A non-convex perspective.". *IEEE Transactions on Circuits and Systems for Video Technology*, 31(3):1103–1113, 2021. DOI: https://doi.org/10.1109/TCSVT.2020.2995866.

[6] J. Wang, J. Liu, and T. Wu. "Level set method for image segmentation model based on improved signed pressure force function.". *Proceedings of the 33rd Chinese Control and Decision Conference, CCDC 2021, Institute of Electrical and Electronics Engineers Inc.*, page 397–400, 2021. DOI: https://doi.org/10.1109/CCDC52312.2021.9601460.

[7] Y. Wang, Z. Wang, and Z. Xie. "A noisy image segmentation method based on improved active contour model.". *2021 IEEE Conference on Telecommunications, Optics and Computer Science, TOCS 2021, Institute of Electrical and Electronics Engineers Inc.*, page 353–356, 2021. DOI: https://doi.org/10.1109/TOCS53301.2021.9688905.

[8] M. Ben Salah, A. Mitiche, and I. Ben Ayed. "Multiregion image segmentation by parametric kernel graph cuts.". *IEEE Transactions on Image Processing*, 20(2):545–557, 2011. DOI: https://doi.org/10.1109/TIP.2010.2066982.

[9] M. A. Guerroudji, K. Amara, D. Aouam, N. Zenati, O. Djekoune, and M. Masmoudi. "Brain tumor segmentation on MRI using a

GVF snake model.". *7th International Conference on Image and Signal Processing and their Applications, ISPA 2022 - Proceedings, Institute of Electrical and Electronics Engineers Inc.*, 2022.
DOI: https://doi.org/10.1109/ISPA54004.2022.9786335.

[10] A. M. Moubark, M. H. Mohd Zaman, M. A. Zulkifley, S. H. Md Ali, L. Nie, and S. Freear. "Despeckling ultrasound B-mode images denoised by a new unsharp masking method for improved cyst segmentation.". *Proceedings - 2020 IEEE EMBS Conference on Biomedical Engineering and Sciences, IECBES 2020, Institute of Electrical and Electronics Engineers Inc.*, page 178–182, 2021.
DOI: https://doi.org/10.1109/IECBES48179.2021.9398839.

[11] O. Lézoray. "Graph signal active contours.". *Proceedings - International Conference on Pattern Recognition, Institute of Electrical and Electronics Engineers Inc.*, page 438–445, 2020.
DOI: https://doi.org/10.1109/ICPR48806.2021.9413213.

[12] C. M. Abid Rahman and H. Nyeem. "A new weighted relative entropy pre-fitting for active contour based image segmentation.". *2019 IEEE International Conference on Signal Processing, Information, Communication and Systems, SPICSCON 2019, Institute of Electrical and Electronics Engineers Inc.*, page 86–89, 2019.
DOI: https://doi.org/10.1109/SPICSCON48833.2019.9065146.

[13] T. Wu, J. Liu, and J. Wang. "Active contour model integrating global and local information.". *IEEE Advanced Information Technology, Electronic and Automation Control*, page 989–993, 2021.
DOI: https://doi.org/10.1109/IAEAC50856.2021.9391022.

[14] Z. Wang, B. Ma, and Y. Zhu. "Review of level set in image segmentation.". *Archives of Computational Methods in Engineering*, 28(4): 2429–2446, 2021.
DOI: https://doi.org/10.1007/s11831-020-09463-9.

[15] Q. Guo, Z. Jiang, H. Wang, M. Yu, and Z. Zhao. "Automatic segmentation of dynamic thyroid ultrasound images based on an improved DRLSE model.". *Proceeding - 2021 China Automation Congress, CAC 2021, Institute of Electrical and Electronics Engineers Inc.*, page 5875–5880, 2021.
DOI: https://doi.org/10.1109/CAC53003.2021.9728139.

[16] Y. Liu et al. "Level set guided region prototype rectification network for retinal vessel segmentation.". *Biomed Signal Process Control*, 87:105428, 2024.
DOI: https://doi.org/10.1016/j.bspc.2023.105428.

[17] Q. Cai et al. "AVLSM: Adaptive Variational Level Set Model for image segmentation in the presence of severe intensity inhomogeneity and high noise.". *IEEE Transactions on Image Processing*, 31: 43–57, 2022.
DOI: https://doi.org/10.1109/TIP.2021.3127848.

[18] V. R. Balaji, S. T. Suganthi, R. Rajadevi, V. Krishna Kumar, B. Saravana Balaji, and S. Pandiyan. "Skin disease detection and segmentation using dynamic graph cut algorithm and classification through Naive Bayes classifier.". *Measurement (Lond)*, 163:107922, 2020.
DOI: https://doi.org/10.1016/j.measurement.2020.107922.

[19] D. Yuan, J. Qiang, J. Li, H. Zhang, and X. Luo. "Figure-ground image segmentation via semantic information.". *2019 IEEE International Conference on Real-Time Computing and Robotics, RCAR 2019, Institute of Electrical and Electronics Engineers Inc.*, page 895–900, 2019.
DOI: https://doi.org/10.1109/RCAR47638.2019.9043955.

[20] D. Y. Nam and J. K. Han. "Improved depth estimation algorithm via superpixel segmentation and graph-cut.". *Digest of Technical Papers - IEEE International Conference on Consumer Electronics, Institute of Electrical and Electronics Engineers Inc.*, 2021.
DOI: https://doi.org/10.1109/ICCE50685.2021.9427631.

[21] M. Hamad, C. Conti, A. M. De Almeida, P. Nunes, and L. D. Soares. "SLFS: Semi-supervised Light-field Foreground-background Segmentation.". *Telecoms Conference, ConfTELE 2021, Institute of Electrical and Electronics Engineers Inc.*, pages 189–194, 2021.
DOI: https://doi.org/10.1109/ConfTELE50222.2021.9435461.

[22] Y. Zhou, G. Gallego, X. Lu, S. Liu, and S. Shen. "Event-based motion segmentation with spatio-temporal graph cuts.". *IEEE Trans Neural Netw Learn Syst*, 34(8):4868–4880, 2023.
DOI: https://doi.org/10.1109/TNNLS.2021.3124580.

[23] U. M. Nunes and Y. Demiris. "Kinematic structure estimation of arbitrary articulated rigid objects for event cameras.". *Proceedings - IEEE International Conference on Robotics and Automation, Institute of Electrical and Electronics Engineers Inc.*, page 508–514, 2022.
DOI: https://doi.org/10.1109/ICRA46639.2022.9812430.

[24] S. Qu, H. Tan, Q. Li, and Z. Peng. "Interactive image segmentation based on the appearance model and orientation energy.". *Computer Vision and Image Understanding*, 217:103371, 2022.
DOI: https://doi.org/10.1016/j.cviu.2022.103371.

[25] M. Wan et al. "Automatic segmentation of coronary artery lumen via anisotropic graph-cuts.". *Proceedings of the Annual International Conference of the IEEE Engineering in Medicine and Biology Society, EMBS, Annu Int Conf IEEE Eng Med Biol Soc*, page 4871–4874, 2019.
DOI: https://doi.org/10.1109/EMBC.2019.8856353.

[26] F. Tian, Y. Gao, Z. Fang, and J. Gu. "Automatic coronary artery segmentation algorithm based on deep learning and digital image processing.". *Applied Intelligence*, 51(12):8881–8895, 2021.
DOI: https://doi.org/10.1007/s10489-021-02197-6.

[27] K. W. Tong, X. Y. Zhao, Y. X. Li, and P. Li. "Individual-level fMRI segmentation based on graphs.". *IEEE Trans Cogn Dev Syst*, 2023.
DOI: https://doi.org/10.1109/TCDS.2023.3281271.

[28] C. Pan, X. Gao, Y. Wang, and J. Li. "Markov random fields integrating adaptive interclass-pair penalty and spectral similarity for hyperspectral image classification.". *IEEE Transactions on Geoscience and Remote Sensing*, 57(5):2520–2534, 2019.
DOI: https://doi.org/10.1109/TGRS.2018.2874077.

[29] Y. Boykov, O. Veksler, and R. Zabih. "Fast approximate energy minimization via graph cuts.". *IEEE Trans Pattern Anal Mach Intell*, 23(11):1222–1239, 2001.
DOI: https://doi.org/10.1109/34.969114.

[30] M. Anousouya Devi, J. I. Sheeba, and K. S. Joseph. "Neutrosophic graph cut-based segmentation scheme for efficient cervical cancer detection.". *Journal of King Saud University - Computer and Information Sciences*, 34(1):1352–1360, 2022.
DOI: https://doi.org/10.1016/j.jksuci.2018.09.014.

[31] J. A. Jeba and S. N. Devi. "Efficient graph cut optimization using hybrid kernel functions for segmentation of FDG uptakes in fused PET/CT images.". *Applied Soft Computing Journal*, 85:105815, 2019.
DOI: https://doi.org/10.1016/j.asoc.2019.105815.

[32] A. Sbei, K. ElBedoui, W. Barhoumi, and C. Maktouf. "Gradient-based generation of intermediate images for heterogeneous tumor segmentation within hybrid PET/MRI scans.". *Comput Biol Med*, 119:103669, 2020.
DOI: https://doi.org/10.1016/j.compbiomed.2020.103669.

[33] Y. Zhang, M. Liu, H. Zhang, G. Sun, and J. He. "Adaptive fusion affinity graph with noise-free online low-rank representation for natural image segmentation.". *Pattern Recognit*, 141:109611, 2023.
DOI: https://doi.org/10.1016/j.patcog.2023.109611.

[34] Y. Han and M. Filippone. "Mini-batch spectral clustering.". *Proceedings of the International Joint Conference on Neural Networks*, 2017-May:3888–3895, 2017.
DOI: https://doi.org/10.1109/IJCNN.2017.7966346.

[35] G. Cheung, E. Magli, Y. Tanaka, and M. K. Ng. "Graph spectral image processing.". *Proceedings of the IEEE*, 106(5):907–930, 2018.
DOI: https://doi.org/10.1109/JPROC.2018.2799702.

[36] S. Piérard et al. "Mixture domain adaptation to improve semantic segmentation in real-world surveillance.". *2023 IEEE/CVF Winter Conference on Applications of Computer Vision Workshops (WACVW)*, page 1–10, 2023.
DOI: https://doi.org/10.1109/WACVW58289.2023.00007.

[37] J. A. Bazerque and G. B. Giannakis. "Nonparametric basis pursuit via sparse kernel-based learning: A unifying view with advances in blind methods.". *IEEE Signal Process Mag*, 30(4):112–125, 2013.
DOI: https://doi.org/10.1109/MSP.2013.2253354.

[38] S. Dambreville, Y. Rathi, and A. Tannenbaum. "A framework for image segmentation using shape models and kernel space shape priors.". *IEEE Trans Pattern Anal Mach Intell*, 30(8):1385, 2008.
DOI: https://doi.org/10.1109/TPAMI.2007.70774.

[39] M. Niazi, K. Rahbar, M. Sheikhan, and M. Khademi. "Customized RBF kernel graph-cut for weak boundary image segmentation.". *Signal Image Video Process*, 17(6):3211–3219, 2023.
DOI: https://doi.org/10.1007/S11760-023-02546-7/METRICS.

[40] F. Martínez, H. Montiel, and F. Martínez. "A novel visual tracking scheme for unstructured indoor environments.". *International Journal of Electrical and Computer Engineering (IJECE)*, 13(6): 6216–6227, 2023.
DOI: https://doi.org/10.11591/ijece.v13i6.pp6216-6227.

[41] L. Lalaoui and T. Mohamadi. "A comparative study of image region-based segmentation algorithms.". *International Journal of Advanced Computer Science and Applications*, 4(6), 2013.
DOI: https://doi.org/10.14569/IJACSA.2013.040627.

[42] D. Martina, C. Fowlkes, D. Tal, and J. Malik. "The berkeley segmentation dataset and benchmark.". 2024. URL https://www2.eecs.berkeley.edu/Research/Projects/CS/vision/bsds/.

[43] M. Everingham, S. M. A. Eslami, L. Van Gool, C. K. I. Williams, J. Winn, and A. Zisserman. "The PASCAL visual object classes homepage.". *PASCAL VOC Project*, 2024. URL http://host.robots.ox.ac.uk/pascal/VOC/.

[44] M. Niazi, K. Rahbar, M. Sheikhan, and M. Khademi. "Customized RBF kernel graph-cut for weak boundary image segmentation.". *Signal Image Video Process*, 17(6):3211–3219, 2023.
DOI: https://doi.org/10.1007/s11760-023-02546-7.

[45] S. Qu, H. Tan, Q. Li, and Z. Peng. "Interactive image segmentation based on the appearance model and orientation energy.". *Computer Vision and Image Understanding*, 217:103371, 2022.
DOI: https://doi.org/10.1016/j.cviu.2022.103371.

[46] G. Weng, B. Dong, and Y. Lei. "A level set method based on additive bias correction for image segmentation.". *Expert Syst Appl*, 185: 115633, 2021.
DOI: https://doi.org/10.1016/j.eswa.2021.115633.

[47] K. Rahbar. "Image segmentation through modeling the illumination probability distribution function using the Krawtchouk polynomial.". *Signal Processing*, 164:1–9, 2019.
DOI: https://doi.org/10.1016/j.sigpro.2019.05.033.

[48] S. Mukherjee and S. T. Acton. "Region based segmentation in presence of intensity inhomogeneity using legendre polynomials.". *IEEE Signal Process Lett*, 22(3):298–302, 2015.
DOI: https://doi.org/10.1109/LSP.2014.2346538.

[49] S. Pang et al. "SpineParseNet: Spine parsing for volumetric MR image by a two-stage segmentation framework with semantic image representation.". *IEEE Trans Med Imaging*, 40(1):262–273, 2021.
DOI: https://doi.org/10.1109/TMI.2020.3025087.

[50] M. S. Alam, D. Wang, and A. Sowmya. "Image data augmentation for improving performance of deep learning-based model in pathological lung segmentation.". *DICTA 2021 - 2021 International Conference on Digital Image Computing: Techniques and Applications, Institute of Electrical and Electronics Engineers Inc.*, 2021.
DOI: https://doi.org/10.1109/DICTA52665.2021.9647209.

[51] A. W. Setiawan. "Image segmentation metrics in skin lesion: Accuracy, sensitivity, specificity, dice coefficient, Jaccard index, and Matthews correlation coefficient.". *CENIM 2020 - Proceeding: International Conference on Computer Engineering, Network, and Intelligent Multimedia 2020, Institute of Electrical and Electronics Engineers Inc.*, page 97–102, 2020.
DOI: https://doi.org/10.1109/CENIM51130.2020.9297970.

[52] K. Ejaz, N. B. M. Suaib, M. S. Kamal, M. S. M. Rahim, and N. Rana. "Segmentation method of deterministic feature clustering for identification of brain tumor using MRI.". *IEEE Access*, 11:39695–39712, 2023.
DOI: https://doi.org/10.1109/ACCESS.2023.3263798.

[53] S. Samudrala and C. K. Mohan. "Semantic segmentation in medical image based on hybrid dlinknet and unet.". *3rd IEEE 2022 International Conference on Computing, Communication, and Intelligent Systems, ICCCIS 2022, Institute of Electrical and Electronics Engineers Inc.*, page 42–47, 2022.
DOI: https://doi.org/10.1109/ICCCIS56430.2022.10037693.